BioChem Press

Inter*net* Electronic Journal of Molecular Design

January 2004, Volume 3, Number 1, Pages 1–10

Editor: Ovidiu Ivanciuc

Special issue dedicated to Professor Nenad Trinajstić on the occasion of the 65th birthday
Part 7

Guest Editor: Douglas J. Klein

Interconversion of Singlet Indium Subhydride Isomers: Theoretical Study

Jerzy Moc and Maria Wierzejewska

Faculty of Chemistry, Wroclaw University, F. Joliot–Curie 14, 50–383 Wroclaw, Poland

Interconversion of Singlet Indium Subhydride Isomers: Theoretical Study[#]

Jerzy Moc* and Maria Wierzejewska

Faculty of Chemistry, Wroclaw University, F. Joliot–Curie 14, 50–383 Wroclaw, Poland

Abstract

Motivation. The recent matrix isolation infrared (IR) studies by Downs and co–workers reported the detection of some indium subhydride In_2H_2 isomers. The dibridged isomer **1** and trans isomer **3** were identified, whereas the experimental IR spectra did not provide any indication of other plausible singlet isomers: branched **2** and monobridged **4**. In order to shed more light on the rearrangement barrier heights and related kinetic stability of various forms of In_2H_2 we have undertaken quantum–chemical study of the isomerization and dissociation pathways and IR spectra of this elusive main–group heavy metal hydride.

Method. Density functional theory (DFT) with B3LYP functional and *ab initio* second–order Møller–Plesset (MP2) perturbation theory were used for structure determination, whereas energetics was evaluated by means of coupled–cluster singles and doubles method incorporating a perturbative correction for triples (CCSD(T)). For indium, Wadt and Hay (WH), Stevens, Basch, Krauss and Jasien (SBKJ) and Stuttgart–Dresden–Bonn (SDB) relativistic effective core potentials (ECP) were employed in conjunction with the appropriate valence basis sets to examine the effect of the ECP/basis on the results.

Results. The reaction pathways for the interconversion of the four isomers **1**–**4** of In_2H_2 have been calculated and the results compared with the experimental data.

Conclusions. The lowest energy rearrangement of the most stable dibridged isomer **1** into the branched **2** and trans **3** isomers occurs via the two step mechanism with the monobridged species **4** involved as the intermediate and the corresponding energy barriers lying in the range ca. 16–20 kcal/mol relative to **1**.

Keywords. Indium subhydride In_2H_2; isomerization pathways; kinetic stability; ECP; vibrational frequencies.

Abbreviations and notations	
CCSD, Coupled–cluster singles and doubles	PES, Potential energy surface
DFT, Density functional theory	TS, Transition state
ECP, Effective core potential	ZPE, Zero point energy

1 INTRODUCTION

Hydrides formed by main group and transition metals have been studied for more than three decades and have attracted considerable attention of both experimentalists and theoreticians [1]. Although many simple hydride molecules can survive long enough to be detected in the gas phase,

most of our experimental knowledge on the hydrides of the main group metals comes from the results of matrix isolation technique. Infrared (IR) and electron paramagnetic resonance (EPR) spectroscopic methods are most often used to detect, identify and characterize a molecule entrapped in a solid inert matrix. A typical strategy is to mix metal atoms or small metal clusters obtained by thermal diffusion or laser ablation with an excess of matrix gas to form a solid condensate at low temperatures. Recently, Himmel *et al*. [2,3] carried out a comprehensive study of the photolytically activated reactions occurring in an Ar matrix between In_2 dimer and H_2. At the first stage of the experiment, these authors identified the In_2H_2 product formed photolytically on deposition of the matrix to be a planar dibridged isomer $In(\mu–H)_2In$. The follow–up irradiation of the matrix with visible light resulted in the rearrangement to a mixture of two species, suggested to be the trans isomer HInInH and InH molecule. The trans HInInH isomer was found to rearrange photolytically back to the dibridged species [2,3].

As far as the quantum chemical studies on In_2H_2 subhydride are concerned, only a few *ab initio* [4] and DFT [2,3] calculations were reported. Treboux and Barthelat [4] investigated periodic trends in the structures and stabilities for the X_2H_2 series with X belonging to the main Group 13. They performed *ab initio* SCF and configuration interaction (CI) calculations, employing effective–core potential (ECP) on heavy atoms and associated valence DZP basis sets. For In_2H_2, the planar dibridged $In(\mu–H)_2In$ (D_{2h}) **1**, branched $InInH_2$ (C_{2v}) **2**, trans HInInH (C_{2h}) **3** and planar monobridged $HIn(\mu–H)In$ (C_s) **4** structures were studied. In aid of their matrix isolation infrared studies, especially to assist in the assignment of the IR spectra of In_2H_2, Himmel *et al*. [2,3] made DFT calculations using B3PW91 functional and ECP on In and the valence DZP basis set. The vibrational frequencies of the partially and fully deuterated forms of In_2H_2 were predicted [2,3].

It is clear from the above review that neither the isomerization reactions of In_2H_2 nor related kinetic stability of its various structures have been addressed so far. Here, the rearrangement pathways of the planar dibridged $In(\mu–H)_2In$ precursor **1** to the other In_2H_2 species are studied. We will show that, on the ground–state singlet potential energy surface (PES) of In_2H_2, the favorable isomerization channels involve transition states lying ca. 16–20 kcal/mol higher than **1**.

2 COMPUTATIONAL METHODS

Initial calculations were performed using density functional theory (DFT) with the B3LYP functional [5,6]. For In, we used relativistic effective–core potential (ECP) of Wadt and Hay (WH) [7] (the large core) in conjunction with the augmented valence (3s3p2d)/[2s2p2d] basis set [7,8] and hydrogen double–zeta polarized (DZP) (4s1p)/[2s1p] set [8,9]. This ECP/basis combination is termed WH. Optimized structures and corresponding energy second derivatives with respect to the nuclear coordinates (hessians) were found in order to provide harmonic vibrational frequencies and zero–point energy (ZPE) corrections. Minima were connected to each transition state (TS) by

tracing the B3LYP/WH intrinsic reaction coordinate (IRC) [10]. Next, all the structures and hessians were recalculated using *ab initio* second–order Møller–Plesset perturbation theory (MP2) [11]. For In, the small core relativistic ECP of Stevens, Basch, Krauss and Jasien (SBKJ) [12] was used in conjunction with the augmented valence (9s9p6d)/[5s5p4d] basis set [12,13] and hydrogen polarized valence triple–zeta 6–311G(p) set [14]. We will refer to this second ECP/basis set as SBKJ. The improved energetics with SBKJ was obtained using coupled–cluster singles and doubles method that includes a perturbative estimate of triples (CCSD(T)) [15]. The justification of using SBKJ and associated more flexible valence basis set (compared to WH) for the *ab initio* correlated calculations was the better description of virtual orbitals involved in the correlation treatment. To assess the effect of the In ECP/basis set on the CCSD(T) energetics, the Stuttgart–Dresden–Bonn (SDB) relativistic ECP (the large core) [16] was also employed together with the augmented correlation–consistent polarized valence triple–zeta (aug–cc–pVTZ) basis set specifically designed for this In ECP [17] and with the aug–cc–pVTZ set for H [18,19]. The latter ECP/basis combination is termed SDB–aug–cc–pVTZ. The calculations were accomplished with Gaussian 98 code [20].

3 RESULTS AND DISCUSSION

In Figure 1, the B3LYP/WH and MP2/SBKJ structures of the **1–4** In_2H_2 isomers and located transition states are displayed, and in Figure 2 the potential energy diagram for the singlet In_2H_2 is shown. The relative energies of all the species and isomerization barrier heights calculated at the B3LYP/WH//B3LYP/WH, CCSD(T)/SBKJ//MP2/SBKJ and CCSD(T)/SDB–aug–cc–pVTZ//MP2/SBKJ levels are presented in Tables 1 and 2. For the purpose of discussion below, the CCSD(T)/SBKJ and CCSD(T)/SDB–aug–cc–pVTZ relative energies, both ZPE–corrected, will be used. Consistent with Table 2 and Figure 2, the number given before (after) slash has been calculated at the CCSD(T)/SBKJ//MP2/SBKJ (CCSD(T)/SDB–aug–cc–pVTZ//MP2/SBKJ) level.

3.1 In_2H_2 Isomers

The planar dibridged isomer $In(\mu–H)_2In$ (D_{2h}) **1** is found to be of lowest energy, in agreement with the reported theoretical findings [3,4]. The branched $InInH_2$ (C_{2v}) **2**, trans HInInH (C_{2h}) **3** and monobridged $HIn(\mu–H)In$ (C_s) **4** isomers are predicted to lie 11.7/14.5, 16.1/19.0 and 10.7/12.0 kcal/mol higher than **1** (Table 1). These relative energies are significantly larger as compared to the ZPE corrected CCSD(T) results for the analogous Ga_2H_2 isomers [21] which placed the **2,3,4** Ga_2H_2 species by 6.8, 12.4 and 7.9 kcal/mol, respectively, above **1**. Despite many trials, we were not able to locate the minimum corresponding to non–planar dibridged structure $In(\mu–H)_2In$ of C_{2v} symmetry ("butterfly" isomer). Our starting "butterfly" structures have invariably collapsed to the planar isomer **1** during geometry optimization at both B3LYP/WH and MP2/SBKJ. The "butterfly" structure is the well documented minimum on the singlet potential energy surface (PES) of X_2H_2

with X=Si,Ge,Sn [22–24] and was recently observed in the gas phase for X=Si [25] and in the solid matrices for X=Ge and Sn [24,26].

H
2.071
[2.042]

3.401[3.339]

In   In

< In-H-In 110.4 [109.7]
1 (D_{2h}) (^1A_g)   planar dibridged

H
1.767
[1.751]

3.129 [3.020]

In   In
109.9
[109.5]

H

2 (C_{2v}) ($^1A_1$)   branched

H
1.805[1.784]

In
3.120 [2.969]

In
118.9
[119.5]

H

3 (C_{2h}) (^1A_g)   trans

H
2.041   2.129
[2.045]   [2.079]

96.0
[92.5]

100.0
[101.6]

H

In   In
3.100 [2.980]

1.789
[1.767]

4 (C_s) ($^1A'$)   monobridged

H
1.689
[1.672]

80.2
[79.3]

In   In
3.444 [3.310]

H

planar dibridged-branched
TS1-2 (C_{2v}) ($^1A_1$)   849 [877] *i*cm^{-1}

H'
87.6
[89.8]

1.834
[1.816]

In   In
3.187 [2.982]

1.941
[1.940] H

2.175[2.136]
Dih In-H-In-H' 94.1 [95.8]

planar dibridged-monobridged
TS1-4 (C_1) (^1A)   300 [280] *i*cm^{-1}

H
1.844
[1.833]

81.1[80.0]

In
3.255 [3.141]

In
1.813
[1.796] H'

< In-In-H' 165.8 [168.0]
trans-monobridged
TS3-4 (C_s) ($^1A'$)   165[158] *i*cm^{-1}

H
1.847[1.847]

73.7
[70.4]

109.3
[109.3]

In   In
2.987 [2.900]

1.752
[1.735] H

branched-monobridged
TS2-4 (C_s) ($^1A'$)   251 [296] *i*cm^{-1}

H A mode
1.838
[1.825]

86.1[87.5]

In   In
3.130 [3.029]

H

Dih H-In-In-H 89.0 [89.8]

SOSP (C_2) (^1A) (A) 281 [257] *i*cm^{-1}
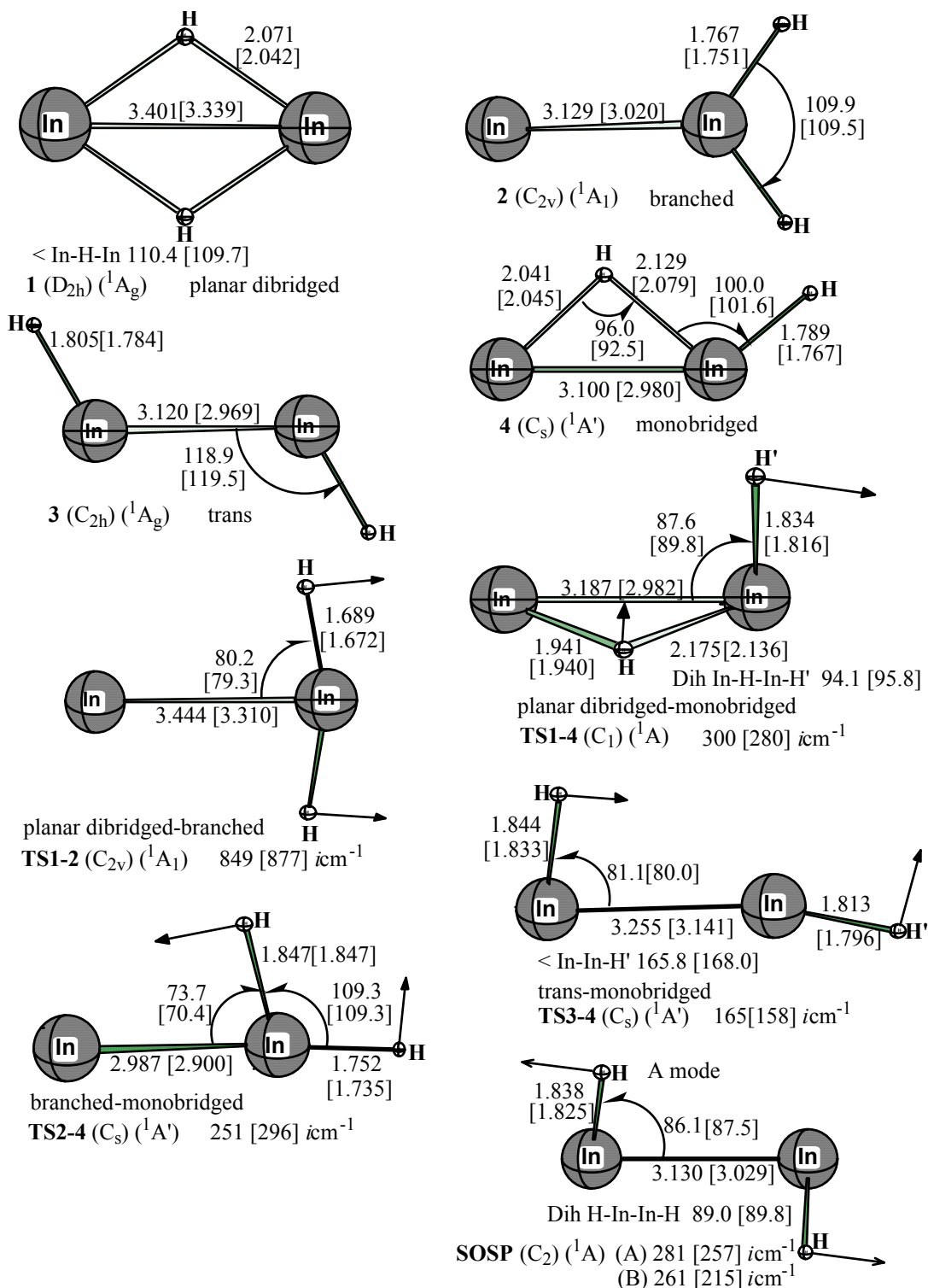   (B) 261 [215] *i*cm^{-1}

Figure 1. Minima and transition states found on the singlet potential energy surface of In$_2$H$_2$ using B3LYP/WH and MP2/SBKJ methods (bond lengths in angstroms, bond angles in degrees); the reaction coordinate vector and the corresponding imaginary frequency are included for each transition state and, for **SOSP**, the A imaginary mode is shown together with both imaginary frequencies. MP2/SBKJ results are given in square brackets.

Table 1. Relative energies (kcal/mol) of the singlet In_2H_2 isomers and isomerization transition states calculated at various computational levels [a]

Species	B3LYP/WH//B3LYP/WH		CCSD(T)/SBKJ//MP2/SBKJ		CCSD(T)/SDB–aug–cc–pVTZ //MP2/SBKJ	
	ΔE	$\Delta E + \Delta ZPE$ [b]	ΔE	$\Delta E + \Delta ZPE$ [c]	ΔE	$\Delta E + \Delta ZPE$ [c]
1(D_{2h}) (^1A_g)	0.0	0.0	0.0	0.0	0.0	0.0
2(C_{2v}) ($^1A_1$)	13.6	14.0	11.2	11.7	14.0	14.5
3(C_{2h}) (^1A_g)	18.2	17.6	16.6	16.1	19.5	19.0
4(C_s) ($^1A'$)	12.1	11.8	11.0	10.7	12.3	12.0
TS1–2(C_{2v}) ($^1A_1$)	52.7	53.2	50.1	50.8	54.9	55.6
SOSP(C_2) (^1A)	22.5	21.2	20.5	19.2	24.0	22.7
TS1–4(C_1) (^1A)	16.4	16.0	14.8	14.5	16.3	16.0
TS2–4(C_s) ($^1A'$)	17.3	17.1	15.5	15.2	17.4	17.1
TS3–4(C_s) ($^1A'$)	19.5	18.4	18.2	17.2	21.3	20.2
2InH	25.4	23.5	25.0	23.0	29.4	27.5

[a] The symbol "//" means "at the geometry of". [b] Using the unscaled B3LYP/WH ZPEs. [c] Using the unscaled MP2/SBKJ ZPEs.

Table 2. Energy barriers (kcal/mol) for the isomerization reactions of singlet In_2H_2 calculated at various computational levels.

Reaction	Barrier [a]	Reaction	Barrier [a]
1 (D_{2h}) → **2** (C_{2v})	50.8/55.6	**2** (C_{2v}) → **1** (D_{2h})	39.1/41.1
1 (D_{2h}) → **4** (C_s)	14.5/16.0	**4** (C_s) → **1** (D_{2h})	3.8/4.0
2 (C_{2v}) → **4** (C_s)	3.5/2.6	**4** (C_s) → **2** (C_{2v})	4.5/5.1
3 (C_{2h}) → **4** (C_s)	1.1/1.2	**4** (C_s) → **3** (C_{2h})	6.5/8.2

[a] The value before slash is from the CCSD(T)/SBKJ//MP2/SBKJ calculation, whereas the value after slash is from the CCSD(T)/SDB–aug–cc–pVTZ//MP2/SBKJ calculation. All the values have been corrected for the respective ZPEs (cf. footnotes under Table 1).

It is seen from Figure 1 that the B3LYP/WH In–In bond lengths in **1**–**4** are found to be consistently longer than the MP2/SBKJ distances, and this holds for the transition structures as well. This trend seems to be caused by the method (B3LYP vs. MP2) rather than the different ECP/basis sets used because the similar behavior was observed for the Ga–Ga bonds in the calculations employing the common basis set [27]. The bonding characteristics of the In_2H_2 species were described elsewhere [4]. Here, our main focus is on prediction of the reaction pathways for their interconversion.

One motivation of this study was the recent matrix isolation IR experiments of In_2H_2 mentioned in the Introduction [2,3]. From the point of view of the experimental observation of different In_2H_2 species, the knowledge of the rearrangement barriers is crucial to determine their kinetic stability. Our calculated isomerization PES is expected to be a useful guide for further experimental studies aiming at the isolation of this heavy metal hydride. In the next section we are addressing the revealed interconversion pathways of In_2H_2.

3.2 Reaction Pathways for the Interconversion of the In$_2$H$_2$ Isomers

The synchronous departing both hydrogens from the dibridged isomer **1** via the C$_{2v}$ symmetry pathway leads to the branched isomer **2** (Figures 1 and 2). This motion causes a simultaneous breaking the two hydrogen bridges and involves the high energy **TS1–2** transition state, lying 50.8/55.6 kcal/mol above **1** (Table 2). It appears that the **1 → 2** isomerization occurring through the concerted mechanism is by far the most energy demanding rearrangement considered in this study (see below). However, we have found that this isomerization can be also accomplished through the energetically much more favorable step–wise mechanism, with the monobridged isomer **4** serving the intermediate. Thus, the first step of the latter mechanism corresponds to the interconversion of **1** into **4** and it is accompanied by breaking the single hydrogen bridge. The characteristic feature of the corresponding **TS1–4** transition structure is that the departing hydrogen makes a dihedral angle with the In–H–In plane being close to 90° (Figure 1). The rearrangement barrier associated with the **1 → 4** step is calculated to be 14.5/16.0 kcal/mol. The follow–up step is the interconversion of the isomer **4** into **2** which proceeds through the planar transition state **TS2–4**. It can be seen from Figure 1 that the corresponding reaction coordinate is the in–plane InH$_2$ rotation. It leads to destroying the second hydrogen bridge and forming the InInH$_2$ isomer **2** (note that the reaction coordinate vector at **TS2–4** in Figure 1 is appropriate for the reverse process). **TS2–4** is placed only 4.5/5.1 and 3.5/2.6 kcal/mol above **4** and **2**, respectively (Table 2).
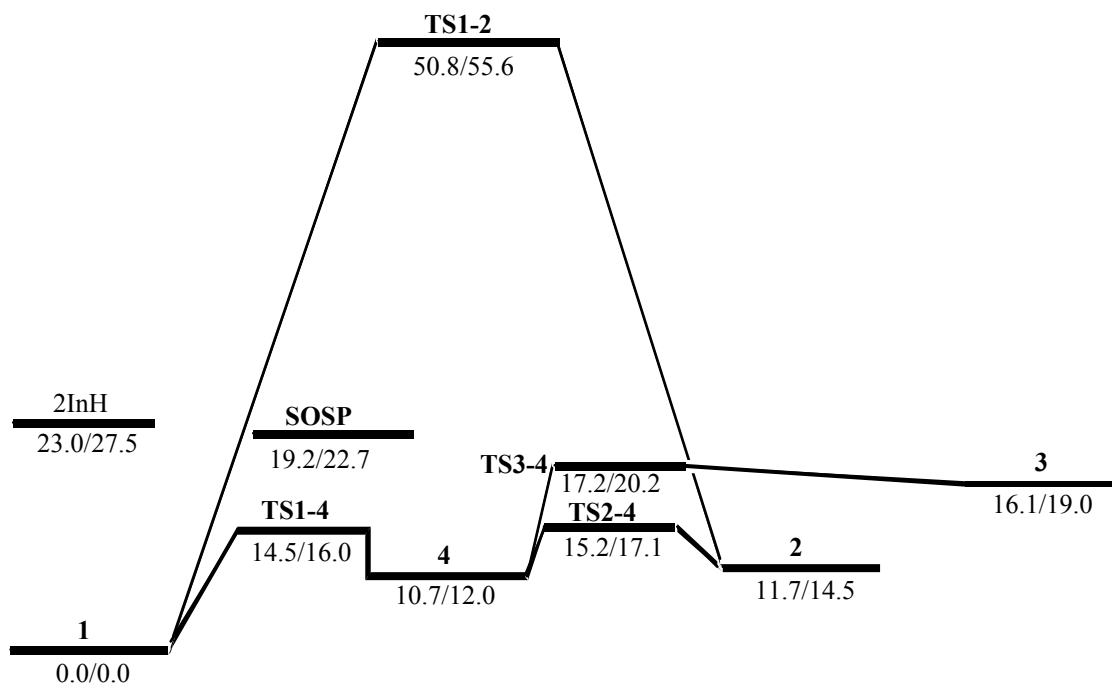

Figure 2. The potential energy diagram for the singlet In$_2$H$_2$. All energies are in kcal/mol; the number given before (after) slash has been calculated at the CCSD(T)/SBKJ//MP2/SBKJ + ZPE (CCSD(T)/SDB–aug–cc–pVTZ//MP2/SBKJ + ZPE) level.

The maximum on the C_2 symmetry path of minimum energy connecting the dibridged isomer **1** and trans isomer **3** corresponds to the second order saddle–point termed **SOSP**. The imaginary mode of A symmetry with the larger (in absolute value) frequency is the C_2–constrained **1** → **3** isomerization coordinate (Figure 1). The constrained barrier height for the interconversion of **1** into **3** is found to be 19.2/22.7 kcal/mol. After relaxing the symmetry constraint in **SOSP**, the structure optimized to the **TS3–4** transition state which connects the minima **3** and **4**. Thus, the HInInH trans isomer **3** can be also obtained from the monobridged species **4**, via **TS3–4** (note that the reaction coordinate vector at **TS3–4** is appropriate for the reverse process). In other words, both step–wise isomerizations of **1** to **2** and **1** to **3** share the intermediate monobridged species **4**. The calculated **4** → **3** rearrangement barrier through **TS3–4** is 6.5/8.2 kcal/mol. For the reverse process, our determined barrier is as small as 1.1/1.2 kcal/mol. This indicates an extremely low kinetic stability of **3** in the gas phase as it transforms back to **4** essentially with no barrier according to our calculations.
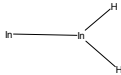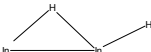
Finally, the two–step rearrangement of the branched isomer **2** into trans isomer **3** with **4** as intermediate can be deduced from Figure 2 (we have not been able to locate a direct transition state for the **2** → **3** rearrangement). By the former mechanism, the isomer **3** is reachable from **2** with the larger barrier corresponding to the **4** → **3** step discussed above.

3.3 Vibrational Frequencies and IR Intensities for the In_2H_2 Isomers

Table 3 summarizes the vibrational frequencies and IR intensities of the four In_2H_2 singlet isomers calculated at B3LYP/WH, MP2/SBKJ and B3PW91 (the latter results taken from Ref. [3]) and those derived from the argon matrix experiments [3]. The contents of Table 3 deserve the following comments. Firstly, all the methods were able to reproduce the intensity pattern of the most stable dibridged isomer **1**. The two modes which have been calculated to have the strongest intensities, $\nu_4(b_{1u})$ and $\nu_5(b_{2u})$, were those actually observed.

The other experimental modes for **1** have been estimated either from the combination bands ($\nu_1(a_g)$ and $\nu_2(a_g)$) or intensified through coupling with the $\nu_5(b_{2u})$ fundamental ($\nu_3(b_{3g})$) [3]. For **3**, only one intense feature is predicted to occur in accord with the measured spectra ($\nu_5(b_u)$). As a matter of fact, the IR identification of **3** was based on this single band. Secondly, the experimental spectra of In_2H_2 did not give any indication of the branched species **2** and monobridged species **4** despite the fact the modes with relatively strong intensity have been found theoretically in both cases (cf. Table 3). Lastly, the DFT findings appear to be in a better overall agreement with experiment than the *ab initio* ones.

Table 3. Comparison of IR spectra calculated and observed for In_2H_2 isomers [a]

Isomer	Calculations			Ar matrix [c]	Assignment
	B3LYP/WH [b]	MP2/SBKJ [b]	B3PW91 [c]		
1				2021, 1079	$\nu_1+\nu_3,\ \nu_2+\nu_3$
	1130 (0)	1204 (0)	1134 (0)	1066.0 [d]	$\nu_1(a_g)$
	1012 (2279)	1069 (2773)	1048 (2268)	954.8	$\nu_4(b_{1u})$
	824 (0)	877 (0)	885 (0)	848 [e]	$\nu_3(b_{3g})$
	802 (228)	858 (283)	808 (244)	800	$\nu_5(b_{2u})$
	301 (3)	273 (11)	333 (6)		$\nu_6(b_{3u})$
D_{2h}	137 (0)	144 (0)	141 (0)	124.3 [d]	$\nu_2(a_g)$
2	1608 (601)	1731 (635)	1602 (607)		$\nu_1(a_1)$
	1608 (368)	1731 (457)	1600 (355)		$\nu_5(b_2)$
	672 (495)	652 (461)	652 (510)		$\nu_2(a_1)$
	311 (80)	341 (94)	304 (74)		$\nu_4(b_1)$
	179 (25)	183 (30)	179 (17)		$\nu_6(b_2)$
C_{2v}	117 (6)	132 (9)	119 (6)		$\nu_3(a_1)$
3	1522 (1187)	1642 (1446)	1518 (1230)	1518	$\nu_5(b_u)$
	1511 (0)	1627 (0)	1505 (0)		$\nu_1(a_g)$
	395 (0)	410 (0)	406 (0)		$\nu_2(a_g)$
	159 (29)	177 (30)	168 (18)		$\nu_4(a_u)$
	135 (31)	133 (49)	152 (36)		$\nu_6(b_u)$
C_{2h}	80 (0)	99 (0)	93 (0)		$\nu_3(a_g)$
4	1542 (786)	1670 (964)	1537 (831)		$\nu_1(a')$
	1023 (357)	1077 (435)	1019 (406)		$\nu_2(a')$
	747 (569)	780 (656)	775 (585)		$\nu_3(a')$
	361 (6)	381 (5)	366 (5)		$\nu_4(a')$
	194 (13)	206 (14)	203 (12)		$\nu_6(a'')$
C_s	92 (4)	113 (6)	102 (5)		$\nu_5(a')$

[a] Frequencies are in cm^{-1}, intensities (in parentheses) in kcalmol^{-1}. [b] This work. [c] Ref. [3]. [d] Value estimated from combination band [3]. [e] Band enhanced through coupling with the $\nu_5(b_{2u})$ fundamental [3].

The reported experimental identification of isomer **3** and not of the more stable (both thermodynamically and kinetically) isomers **2** and **4** requires an additional explanation. In certain instances, a comparison of the gas phase theoretical findings with those derived from the low temperature matrix experiments must be considered with care. This is especially true when the new products, such as the isomer **3**, are generated in the matrix cage and not during the deposition from the gas phase. There are examples in the literature of the less stable structures formed in the matrixes and favored over those being thermodynamically more stable [28,29].

4 CONCLUSIONS

The pathways for the interconversion of **1**–**4** isomers of In_2H_2 have been predicted using DFT and correlated *ab initio* methods and several In relativistic ECP/valence basis set combinations. In accordance with the recent matrix isolation IR studies [2,3] we found dibridged $In(\mu–H)_2In$ isomer **1** to be the most stable thermodynamically and kinetically. The most favorable path leading from **1** to the branched $InInH_2$ form **2** and trans HInInH form **3** involves the two–step mechanism with the monobridged $HIn(\mu–H)In$ form **4** as the intermediate. The transition states involved in the two–step

pathways are placed ca. 16–20 kcal/mol above **1**. The largest revealed energy requirement, for the concerted rearrangement of **1** into **2** via **TS1–2**, is found to be more than twice that needed for the dissociation of **1** into two InH fragments (Table 1).

Acknowledgment

5 REFERENCES

[1] S. Aldridge and A. J. Downs, Hydrides of the Main–Group Metals: New Variations on an Old Theme, *Chem. Rev.* **2001**, *101*, 3305–3365.

[2] H.–J. Himmel, L. Manceron, A. J. Downs and P. Pullumbi, Characterization and Photochemistry of the Gallium and Indium Subhydrides Ga_2H_2 and In_2H_2, *Angew. Chem. Int. Ed.* **2002**, *41*, 796–799.

[3] H.–J. Himmel, L. Manceron, A. J. Downs and P. Pullumbi, Formation and Characterization of the Gallium and Indium Subhydride Molecules Ga_2H_2 and In_2H_2: A Matrix Isolation Study, *J. Am. Chem. Soc.* **2002**, *124*, 4448–4457.

[4] G. Treboux and J.–C. Barthelat, X–X Direct Bonds versus Bridged Structures in Group 13 X_2H_2 Potential Energy Surfaces, *J. Am. Chem. Soc.* **1993**, *115*, 4870–4878.

[5] A. D. Becke, Density–Functional Thermochemistry. III. The Role of Exact Exchange, *J. Chem. Phys.* **1993**, *98*, 5648–5652.

[6] C. Lee, W. Yang and R. G. Parr, Development of the Colle–Salvetti Correlation–Energy Formula into a Functional of the Electron Density, *Phys. Rev. B* **1988**, *37*, 785–789.

[7] W. R. Wadt and P. J. Hay, Ab Initio Effective Core Potentials for Molecular Calculations. Potentials for Main Group Elements Na to Bi, *J. Chem. Phys.* **1985**, *82*, 284–298.

[8] S. Huzinaga, J. Andzelm, M. Klobukowski, E. Radzio–Andzelm, Y. Sakai and H. Tatewaki, *Gaussian Basis Sets for Molecular Calculations*, Elsevier, New York, 1984.

[9] T. H. Dunning and P. J. Hay, Gaussian Basis Sets for Molecular Calculations; in: *Modern Theoretical Chemistry*, Vol.3, Ed. H. F. Schaefer, III, Plenum, 1976, New York, pp 1–27.

[10] C. Gonzalez and H. B. Schlegel, An Improved Algorithm for Reaction Path Following, *J. Chem. Phys.* **1989**, *90*, 2154–2161.

[11] J. A. Pople, J. S. Binkley, R. Seeger, Theoretical Models Incorporating Electron Correlation, *Int. J. Quantum Chem. Symp.* **1976**, *10*, 1–19.

[12] W. J. Stevens, M. Krauss, H. Basch and P. G. Jasien, Relativistic Compact Effective Potentials and Efficient, Shared–Exponent Basis Sets for the Third–, Fourth–, and Fifth–Row Atoms, *Can. J. Chem.* **1992**, *70*, 612–630.

[13] F. R. Bennett and J. P. Connelly, Theoretical Study of the Properties of $InMH_6$ and MBH_6 (M = B, Al, Ga, and In) μ–Hydrido–Bridged Compounds, *J. Phys. Chem.* **1996**, *100*, 9308–9313.

[14] R. Krishnan, J. S. Binkley, R. Seeger and J. A. Pople, Self–Consistent Molecular Orbital Methods. XX. A Basis Set for Correlated Wave Functions, *J. Chem. Phys.* **1980**, *72*, 650–654.

[15] K. Raghavachari, G. W. Trucks, J. A. Pople and M. Head–Gordon, A Fifth–Order Perturbation Comparison of Electron Correlation Theories, *Chem. Phys. Lett.* **1989**, *157*, 479–483.

[16] A. Bergner, M. Dolg, W. Kuchle, H. Stoll and H. Preuss, Ab Initio Energy–Adjusted Pseudopotentials for Elements of Groups 13–17, *Mol. Phys.* **1993**, *80*, 1431–1441.

[17] J. M. L. Martin and A. Sundermann, Correlation Consistent Valence Basis Sets for Use with the Stuttgart–Dresden–Bonn Relativistic Effective Core Potentials: The Atoms Ga–Kr and In–Xe, *J. Chem. Phys.* **2001**, *114*, 3408–3420.

[18] T. H. Dunning, Gaussian Basis Sets for Use in Correlated Molecular Calculations. I. The Atoms Boron through Neon and Hydrogen, *J. Chem. Phys.* **1989**, *90*, 1007–1023.

[19] R. A. Kendall, T. H. Dunning and R. J. Harrison, Electron Affinities of the First–Raw Atoms Revisited. Systematic Basis Sets and Wave Functions, *J. Chem. Phys.* **1992**, *96*, 6796–6806.

[20] M. J. Frisch, G. W. Trucks, H. B. Schlegel, G. E. Scuseria, M. A. Robb, J. R. Cheeseman, V. G. Zakrzewski, J. A. Montgomery, Jr., R. E. Stratman, J. C. Burant, S. Dapprich, J. M. Millam, A. D. Daniels, K. N. Kudin, M. C. Strain, O. Farkas, J. Tomasi, V. Barone, M. Cossi, R. Cammi, B. Mennucci, C. Pomelli, C. Adamo, C. Clifford, J. Ochterski, G. A. Petersson, P. Y. Ayala, Q. Cui, K. Morokuma, D. K. Malick, A. D. Rabuck, K. Raghavachari, J.

B. Foresman, J. Cioslowski, J. V. Ortiz, B. B. Stefanov, G. Liu, A. Liashenko, P. Piskorz, I. Komaromi, R. Gomperts, R. L. Martin, D. J. Fox, T. Keith, M. A. Al–Laham, C. Y. Peng, A. Nanayakkara, C. Gonzalez, M. Challacombe, P. M. W. Gill, B. Johnson, W. Chen, M. W. Wong, J. L. Andres, M. Head–Gordon, E. S. Repogle and J. A. Pople, *Gaussian 98*, *Revision A.1x*, Gaussian, Inc., Pittsburgh, PA, 2001.

[21] Z. Palagy, H. F. Schaefer and E. Kapuy, Ga_2H_2: Planar Dibridged, Vinylidene–Like, Monobridged, and Trans Equilibrium Geometries, *Chem. Phys. Lett.* **1993**, *203*, 195–200.

[22] B. T. Colegrove and H. F. Schaefer, Disilyne (Si_2H_2) Revisited, *J. Phys. Chem.* **1990**, *94*, 5593–5602.

[23] Z. Palagy, H. F. Schaefer and E. Kapuy, Ge_2H_2: A Molecule with a Low–Lying Monobridged Equilibrium Geometry, *J. Am. Chem. Soc.* **1993**, *115*, 6901–6903.

[24] X. Wang, L. Andrews, G. V. Chertihin and P. F. Souter, Infrared Spectra of the Novel Sn_2H_2 Species and the Reactive $SnH_{1,2,3}$ and $PbH_{1,2,3}$ Intermediates in Solid Neon, Deuterium, and Argon, *J. Phys. Chem. A* **2002**, *106*, 6302–6308.

[25] M. Bogey, H. Bolvin, M. Cordonnier, C. Demuynck, J. L. Destombes and A. G. Csaszar, Milimiter– and Submilimiter–Wave Spectroscopy of Dibridged Si_2H_2 Isotopomers: Experimental and Theoretical Structure, *J. Chem. Phys.* **1994**, *100*, 8614–8624.

[26] X. Wang, L. Andrews and G. P. Kushto, Infrared Spectra of the Novel Ge_2H_2 and Ge_2H_4 and the Reactive $GeH_{1,2,3}$ Intermediates in Solid Neon, Deuterium and Argon, *J. Phys. Chem. A* **2002**, *106*, 5809–5816.

[27] N. Takagi, M. W. Schmidt, and S. Nagase, Ga–Ga Multiple Bond in $Na_2[Ar^*GaGaAr^*](Ar^*=C_6H_3-2,6-(C_6H_2-2,4,6-i-Pr_3)_2)$, *Organometallics* **2001**, *20*, 1646–1651.

[28] G. Schatte, H. Willner, D. Hoge, E. Knösinger, O. Schrems, Selective Trapping of the Complexes [OC…HF] and CO…HF] by Photodissociation of Matrix–Isolated Formyl Fluoride, *J. Phys. Chem.* **1989**, *93*, 6025–6028.

[29] J. Lundell, M. Rasänen, The 193 nm Induced Photodecomposition of HCOOH in Rare Gas Matrices: The H_2O–CO 1:1 Complex, *J. Phys. Chem.* **1995**, *99*, 14301–14308.